STOP THAT CORROSION - IF YOU CAN

by Zin Tun, Jamie Noël and Dave Shoesmith

In Spring 1836, Michael Faraday received a letter from Prof. Schoenbein, Professor of Chemistry at the University of Bâle [1]. Schoenbein lamented how slow German periodicals were in getting scientific papers published, and apologized for taking the liberty of writing directly to Faraday. Schoenbein further presented observations he had made recently by dipping iron wires into a strong nitric acid where, under certain conditions, iron seemed to be fully protected from the acid. Faraday repeated Schoenbein's experiments for verification, carried out investigations of his own, and proposed tentatively that the passivation of iron was caused by the growth of a thin oxide layer on the wire. This body of work was published in the Philosophical Magazine [2] later in the year.

The scientific study of passive oxide on metals thus started continues to this day. It is fair to question if there is anything more to discover in such an old area of research. After all, we now know Faraday's proposal is basically correct [3]. The continued interest in the phenomenon is due to several factors, each providing a compelling reason. First, the problem is interesting in its own right, involving the not well-understood solid-state ion transport. Also there remains some fundamental issues not fully resolved. For instance, even the composition and structure of the oxide are still matters of controversy [3]. Second, we all realize that metal passivity, if it were fully understood and controlled, would have major impact, not only for industry but for the whole society. This promise drives researchers to continue looking for a unifying model or explanation, such as a recipe for growing an passive oxide that would effectively stop corrosion of *any* metal under *any* environmental condition. We are fully aware that a general recipe may not exist given that intrinsic properties of metals (alloys included) and their oxides vary enormously. Nevertheless, even if we do not achieve such a lofty goal, the research will still be worthwhile since we will no doubt come across some interesting phenomena as we work in this rich field of research. Finally, the very fact that a thin layer of atoms, often not more than 10 crystallographic unit cells if it were an ordered structure, is capable of stopping this omnipresent agent of destruction - corrosion - is intriguing. It has captured many researchers' interest in the past and is likely to do so in the foreseeable future.

The scientific study of passive oxide on metals started in 1836 continues to this day. It is fair to question if there is anything more to discover in such an old area of research. After all, we now know Faraday's proposal is basically correct [3].

CHANCE FAVOURS THE PREPARED MIND, BUT ...

The chance of observing an interesting phenomenon increases if one uses a new experimental technique, especially if the technique offers some unique capabilities. This brings us to the topic of this article. At Chalk River we have an ongoing research program to study passive oxide layers with neutron reflectometry (NR). Instead of iron, our experiments have been on titanium (Ti) and zirconium (Zr), two metals that are of interest to the nuclear industry.

NEUTRON REFLECTOMETRY

NR is a relatively new neutron scattering technique that allows determination of near-surface layer structure of a flat sample to a resolution of 1 or 2 nanometers in the direction normal to the sample. As the measurements are limited to small scattering angles, individual atoms are not observed by NR. Instead, data analysis yields a function known as the scattering-length density (SLD). The SLD is the product of coherent neutron scattering-length (usually denoted by b) and number density of constituent isotopes of a particular layer. If a layer contains more than one isotope, the layer SLD is the all-inclusive sum performed over all isotopes present. We herein report specular reflectivity measurements where the scattering vector **q** is kept perpendicular to the surface of the sample, taken to be the z-direction. Consequently, specular reflectivity provides no in-plane sensitivity. The SLD profiles we report are functions of z only, and they are the xy-sum of SLD contributed by all isotopes that lie at the particular depth z.

Neutron scattering cross-sections are small compared to those that give rise to X-ray or electron diffraction. Consequently, diffraction signals from a nanometer scale layer would be too weak to measure with neutrons. NR overcomes this difficulty by making use of total external reflection of neutrons when they strike the sample surface at a small enough grazing angle. Just as for visible light, below the critical angle, θ_c, the reflectivity of the interface is unity, *i.e.* the entire incident beam is reflected. Once the grazing angle exceeds θ_c, the reflectivity drops quickly but this drop can be measured with great precision for at least 5 or 6 orders of magnitude. The details of this drop are what conveys the information about the layer structure. For instance, for a sharp interface between two different media, the drop follows the well

Z. Tun <zin.tun@nrc-cnrc.gc.ca>, National Research Council, Chalk River, ON K0J 1J0; J. Noël and D. Shoesmith, Dept.. of Chemistry, Western Ontario, London, ON N6A 5B7

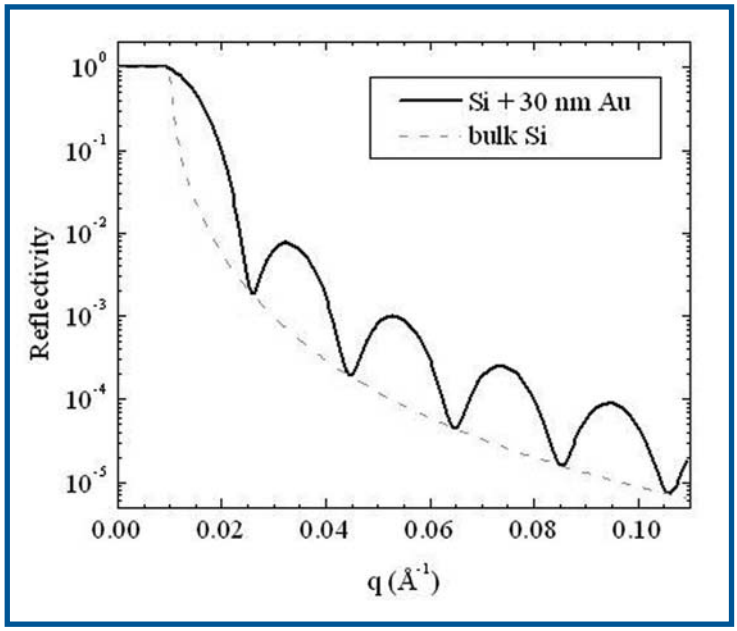

Fig. 1 **Fresnel equation (dashed curve) plotted as a function of the scattering vector q. This is the expected variation of reflectivity if the interface causing the reflection is a sharp boundary between two media. For this plot we assume the media to be air and Si. In the case where there is a thin layer of a third material on the surface (assumed to be Au for this example) an interference pattern will be observed (solid curve).**

known Fresnel equation. In the case of a more complicated example, if the sample consists of several layers, each with a well defined thickness and SLD, an interference pattern appears superimposed on the Fresnel Law (Figure 1). Broad interfaces, in general, can be thought of as a series of "micro-layers" whose SLD follows a profile defined by a sigmoidal function of a finite width. For data analysis, one proposes a layer profile model whose calculated reflectivity is at least approximately similar to the observed reflectivity. Much in the same way as for crystallographic structure refinement, the residual discrepancies between R_{obs} and R_{cal} are then minimized by least-squares refinement of the model parameters, *i.e.* the thickness, SLD, and interface width of the layers are refined.

One advantage of NR that is very much relevant to our research is its ability to detect the presence of hydrogen or H-containing species. ^{1}H (or natural H which is 99.99% ^{1}H) is one of the few isotopes whose neutron scattering length, b, is negative, meaning the Fermi pseudo potential between a proton and a neutron is attractive instead of repulsive. Therefore, during an experiment where an *in-situ* chemical reaction is in progress, a decrease in the SLD of a layer, for example, may signal H ingress into a layer. One can verify this tentative result by repeating the experiment in a deuterated environment, for ^{2}H (or D), unlike H, has a very large positive b. If the hypothesis about the H-ingress is correct, the SLD of the layer should increase in the deuterated experiment.

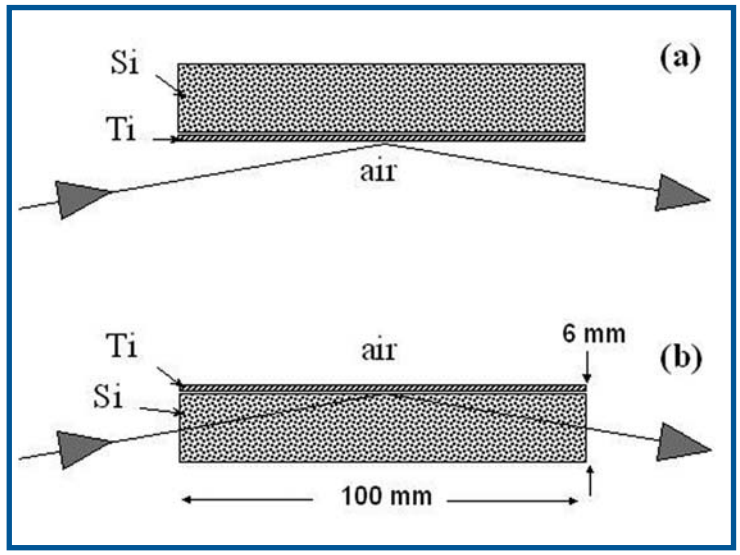

Fig. 2 **Two possible geometries of performing neutron reflectometry on a thin metal film (e.g. Ti film of several tens of nanometers) deposited on a Si substrate. The circular substrate of 100 mm diameter and 6 mm thickness is shown edge-on, and the arrows represent incoming and reflected neutron beams.**

Another advantage of NR is that the scattering geometry makes it particularly easy to combine NR with many other experimental techniques. The $\theta/2\theta$ scan performed for NR is almost a straight-through geometry (often $2\theta < 10^o$), providing un-obscured frontal view of the sample surface and direct access for other probes for simultaneous investigation. The geometry is depicted in Figure 2a. On the other hand, if the sample needs to be enclosed in a special environment (controlled humidity, high vacuum, *etc.*) one can easily design an enclosure with two small windows. Yet another possibility is to use a substrate that is highly transparent to neutrons to support the thin film sample. Most popular substrates are Si or sapphire. In that case, the beam can be arranged to strike the thin-film sample from the substrate side as shown in Figure 2b. Note that the space away from the neutron beams is then entirely clear and open for whatever experiments one wishes to perform simultaneously. Figure 3 is an example of such an experiment where a specially designed cell allows simultaneous performance of NR and electrochemistry on a working electrode. These possibilities make NR very versatile and have produced many ingenious experiments worldwide.

PASSIVE OXIDE ON Ti

Using a cell based on the same design as the one depicted in Figure 3, Wiesler & Majkrzak [4,5] carried out NR on a Ti thin film in contact with (0.1 mole/dm^3) H_2SO_4 solution. In this pioneering work, the authors grew anodic oxide on the already existing passive oxide in two ways – either by applying anodic potential abruptly or by slowly ramping (1 mV/s) the potential to its final value. They found that slightly denser packing results if the potential is slowly ramped, and the denser oxide thus formed dissolves slower in the acid. They also made observations on the loading of H into the oxide and the underlying metal by reversing the bias to cathodic polarity.

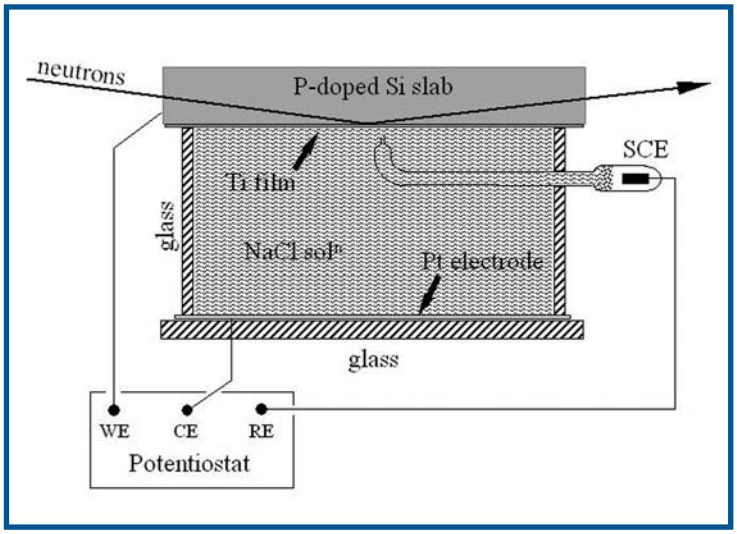

Fig. 3 Schematic of a cell to perform neutron reflectometry and electrochemical reactions simultaneously. The working electrode (WE) is a metal thin film deposited on low-resistance Si, while a Pt foil serves as the counter electrode (CE). A saturated calomel electrode (SCE), connected to the main body of electrolyte via a capillary and a porous ceramic junction acts as the reference electrode (RE) of the cell.

In the 1990s, research groups at AECL's Whiteshell Laboratories had a strong interest in the corrosion properties of Ti because the metal was being considered as a container material for underground spent nuclear fuel disposal (Canadian Nuclear Fuel Waste Management Program). Wiesler & Majkrzak's work inspired us and we set out to do similar NR experiments combined with in-situ electrochemistry. However, there is one major difference: instead of H_2SO_4 we chose to work with aqueous NaCl solution (0.27 mole/dm^3) as the containers would come into contact with near-neutral pH, saline underground water. In addition to a better understanding of the corrosion mechanism, we needed a good estimate of the threshold polarization that would initiate H adsorption into Ti. Our results have been reported in several papers [6-8]. One of the highlights of the work is being able to shed light on the mechanism of ion transport across an existing oxide layer during anodization.

Figure 4 shows the SLD curves of the Ti film exposed to the electrolyte solution both before (*i.e.* at the open circuit potential, E_{OC}) and after being anodized to E = 2 V. Ti is another one of the few isotopes with negative scattering length, and hence the SLD of the metal layer is below zero. The scan at 2 V was performed several hours after setting the potential to ensure we measured the long time equilibrium behaviour of the oxide layer. As expected, the oxide layer, originally at t_{OC} = 47 Å, thickened to t_E = 112 Å by anodization, and used up some 38 Å of the underlying metal in the process. These changes correspond to anodization ratio $\alpha = (t_E - t_{OC})/(E - E_{OC}) = 25.4$ Å/V and the Pilling Bedworth ratio (volume of oxide produced per volume of metal consumed) $R_{PB} = 1.72 \pm 0.04$. These values compare well with literature values: the most commonly accepted value for α for Ti is 25 ± 5 Å/V [9], while R_{PB}, depending on the crystallographic structure of the oxide, is expected to be 1.77, 1.82, and 1.96, respectively, for rutile, brookite and anatase structures. We note that the observed R_{PB} was very low, barely acceptable compared to the formation of rutile, the highest density form of TiO_2. This suggests the resultant oxide was free of major voids and cavities.

Another important result depicted by Figure 4, as deduced from least-squares refinement with various models, is that the outer layer of the anodized oxide (*i.e.* the part that was in contact with the electrolyte) has a lower SLD than the original oxide. Three possibilities present themselves to explain the low SLD region: a) this region of oxide is porous, b) it is oxygen deficient, *i.e.* TiO_x with x < 2, or c) it contains some form of hydrogen. Possibility a) can be ruled out on the basis that the observed R_{PB} is very low, indicating the resultant oxide is highly compact. Since the Ti oxides are insoluble in water, an argument such as "R_{PB} is actually high but it appears low as part of the oxide had dissolved away before NR was started" is not credible. Possibility b) can be rejected on the grounds that oxygen deficiency, if any, should occur deep within the oxide layer, not on the surface. This leaves possibility c) which is most likely since incorporation of H (as OH species) during anodization is indeed a known phenomenon (*e.g.* the observation of absorbed OH by angle resolved XPS as reported by Tun *et al.* [8]).

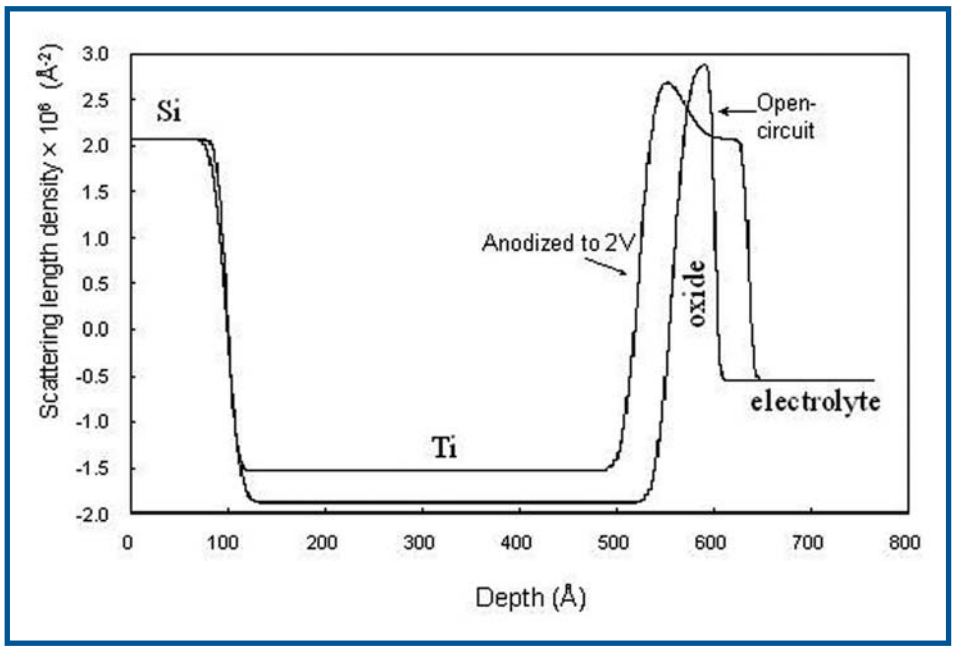

Fig. 4 Scattering-length density (SLD) profile of a Ti thin-film deposited on a Si substrate. The SLD of the metal layer is negative since the scattering length of Ti is negative. The oxide layer, 47 Å prior to anodization (open-circuit E_{OC} = – 0 56 V), thickened to 112 Å after acquiring equilibrium at 2 V applied potential.

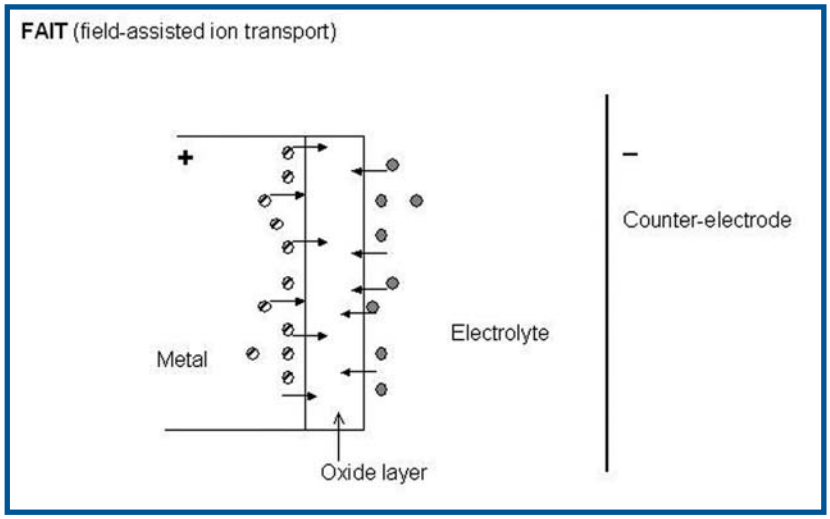

Fig. 5 Visualization of field-assisted ion transport across an existing oxide layer. Most of potential drop between the metal of anode and cathode takes place within the oxide which is an insulator or a large-gap semiconductor. The resulting electric field within the oxide layer drives cations and anions in opposite directions.

Having thus explained the low SLD region, we are confronted with yet another question: Is the high SLD region the original oxide? From the peak value of SLD and the thickness, the high SLD region seems to be very similar to the original oxide; it is tempting to think that they are one and the same. One could argue that the high SLD region is the original oxide that has "sunk" closer to the Si/Ti interface because some amount of metal has been removed and transported across the original oxide to form new oxide (the low SLD region) at the oxide/electrolyte interface. Note also that this consideration is valid regardless of which of the three possibilities as explained above is responsible for the low SLD region. However, such an interpretation is not consistent with known transport numbers for anodization of Ti. Exclusive outward growth of the oxide would require very high Ti mobility. Using α-particle emitters implanted prior to anodization, Khalil and Leach [10] determined from the energy-loss spectrum that the emitter layer was buried within the thickened anodized oxide, at a depth of 35% of the increase in the oxide layer thickness. This corresponds to 35% metal and 65% oxygen mobility. Clearly, an alternative explanation is needed.

It is important to first recognize that our desire to talk about the original oxide comes from the field-assisted ion transport (FAIT) model. The basic concept of this mechanism is depicted in Figure 5. Differently charged ions migrate through an existing oxide and react with respective counter ions at the metal/oxide or oxide/liquid interface. According to this simple-minded picture of FAIT, the original air grown oxide is merely a passive screen.

Within the FAIT, we are then led to the following picture at the molecular level: What is attracted towards the anode is OH. Presumably H is stripped by the very large potential gradient within the existing oxide, H remains within the shallower depths while O continues to pass through (with 65% mobility), and react with Ti. Meanwhile, Ti migrates out (with 35% mobility) and reacts with O (as OH or water) at the oxide/electrolyte interface. Thus we end up with an inner layer of H-free oxide and an outer layer of H-containing oxide. If we accept this picture of oxide growth, the fact that the H-containing region ends just at the right depth so that the H-free region happens to have the same thickness as the original air-grown oxide is an accident. While there is nothing preventing such a fortuitous outcome, we thought it was desirable to look for alternative models of solid-state oxide growth where the amount of H-free oxide is necessarily conserved.

The alternative model we favour is the point-defect model (PDM) [11]. The basic idea is depicted in Figure 6. According to this model, field-driven migration of one of the species, say O, is initiated when an O atom near the metal/oxide layer hops into a defect site in the metal. This creates a vacancy in the oxide, which is filled by an O atom at a shallower depth of the oxide, leaving its original site vacant. This sequence of vacancy creation and subsequent filling by a nearby ion propagates outward through the existing oxide until, finally, the vacancy created at the oxide/liquid interface is filled by an O atom (or an OH ion) derived from the solution. The metal ions can also migrate through the existing oxide by a similar vacancy transfer process running in the opposite direction.

The O in the original air-grown oxide is H-free and, since this number of O atoms is conserved according to PDM, the thickness of H-free oxide would be conserved. The newly incorporated O by anodization is contaminated to some extent with H, causing the extra thickness of the oxide produced by anodization to have a lower SLD. The fact that we do not need to invoke a fortuitous outcome makes the PDM more attractive. However, we recognize that a more direct experimental evidence is needed to decidedly settle this issue.

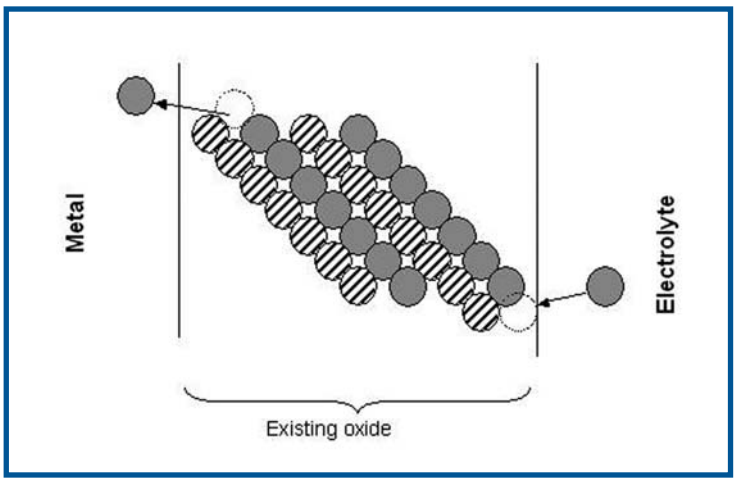

Fig. 6 Visualization of point-defect model of ion transport. When an ion within the existing oxide hops to a neighbouring lattice vacancy (defect), it creates a vacancy at its original site.

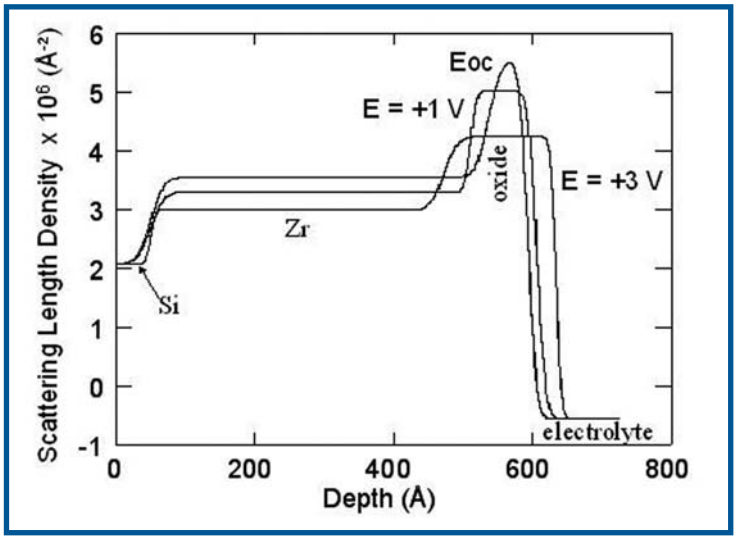

Fig. 7 Scattering-length density (SLD) profile of a Zr thin-film deposited on a Si substrate before anodization (labeled EOC), after attaining equilibrium at 1 V (E = +1V) and subsequently at 3 V (E = +3V).

Repeating NR with a solution made of D_2O instead of H_2O may provide further evidence, but a fresh look with an entirely different technique may provide a more convincing outcome.

PASSIVE OXIDE ON Zr

Another metal that is of interest to the nuclear industry is Zr. Our studies of Zr are more extensive than those on Ti since we managed to carry out electrochemical impedance spectroscopy (EIS) concurrently with NR. Combining NR and EIS, though simple in theory, is very challenging because of electrical interference. Following the time-honoured approach of trial and error, we learned not only that the cell must be electrically isolated from the common ground of the neutron instrumentation, but also that no metal part of the cell must come close (within about 2 inches) to any grounded object (*e.g.* the top metal plate of the θ rotary drive) even when these parts themselves are electrically isolated from the EIS circuit.

EIS is a familiar technique for electrochemists. By superimposing a small AC ripple of variable frequency on the DC bias applied for anodic or cathodic polarization of the working electrode, the AC response of the electrode (*i.e.* current) is recorded over a frequency range spanning from a few mHz to ~100 kHz. Currents as low as a few nano-amperes are recorded. The data are then analyzed in terms of an equivalent circuit where a capacitor, for example, would represent the charge storage capacity of the double-layer on the electrode surface and a resistor parallel to it would represent charge leakage whose origin could be an electrochemical reaction or an electronic or ionic current. Only a preview of our NR and EIS results is provided here as we intend to publish a full account of these experiments elsewhere.

The SLD curves of our Zr thin film sample obtained at open circuit (E_{OC} = –0.17 V) and two anodizing potentials are shown in Figure 7. Actually, NR (and EIS) data were collected at anodic potentials starting from 0 to 3 V in steps of 0.5 V. To ensure long time equilibrium behaviour was recorded, the NR scans, each typically taking 6 h, were repeated until no further change was discernable in the measured reflectivity. Depending on whether the NR scan was initiated immediately after the potential was applied or delayed by several hours, it took two or three repeats to achieve stability. EIS scans were always started immediately after setting the

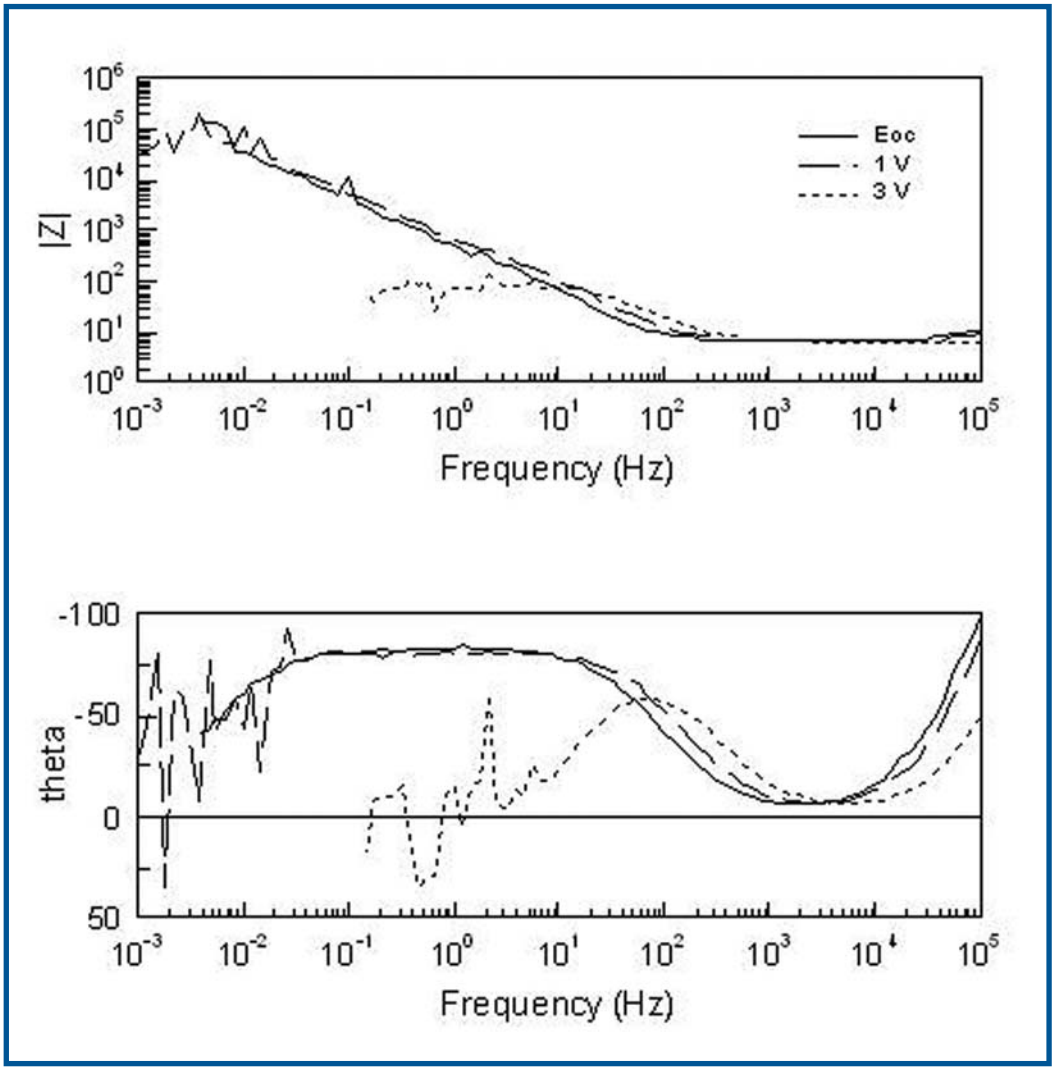

Fig. 8 Impedance of the thin-film Zr electrode before it was anodized (labeled EOC), and after being anodized to a potential of 1 V (1V) and 3 V (3V).

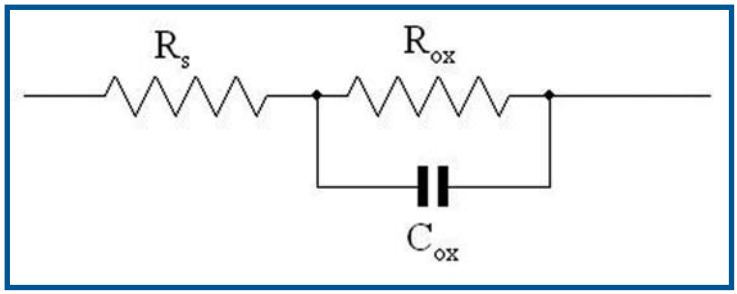

Fig. 9 Equivalent circuit proposed for the analysis of observed frequency dependence of Zr electrode impedance.

potential. Each typically taking ~ 2 h to complete, we collected 12 to 18 completed EIS scans at each potential.

Just as Figure 4 does for Ti, Figure 7 shows thickening of oxide at the expense of the Zr metal. The numerical values of α and R_{PB}, 34 Å/V and 1.57 respectively, are in good agreement with the literature values [12,13]. However, a two-oxide model such as that used for the anodized Ti oxide does not give a stable or significantly improved least-squares refinement at any of the potentials where we have made measurements. We concluded that there is no basis for invoking two types of oxide, and adopted a single oxide layer throughout for reporting the NR results.

The impedance of the cell as measured by EIS at the same three potentials is shown in Figure 8. While many equivalent circuits with different levels of sophistication could be proposed, the circuit shown in Figure 9 is one of the simplest for an electrochemical cell. It consists of a capacitor, C_{ox}, to represent charge storage capacity across the oxide layer and a parallel resistor, R_{ox}, included to model possible charge leakage. The series resistor R_s represents the solution (electrolyte) resistance. For a good insulating oxide layer and an ionic solution such as the one we used $R_{ox} >> R_s$. At the lowest frequency (almost DC), C_{ox} is not conducting since its magnitude of impedance $1/\omega C \rightarrow \infty$, and we essentially have the two resistors R_{ox} and R_s in series. We identify $|Z| \approx R_{ox}$, and expect the phase, Θ, to be zero. As the frequency increases, C_{ox} begins to conduct making the $|Z|$ fall and $\Theta \rightarrow -90^\circ$. Once C_{ox} is fully conducting (frequency ~ 0.1 Hz) the circuit is essentially R_s and C_{ox} in series, whose real part is R_s and the imaginary part $(-\iota/\omega C_{ox})$. As the frequency increases further, the real part remains constant but the imaginary part decreases. Eventually, as the imaginary part becomes comparable to, and then smaller than R_s in magnitude, Θ rotates back from -90° to zero and $|Z| \approx R_s$.

Figure 10 shows the impedance Z of the equivalent circuit whose components R_s, R_{ox} and C_{ox} have been adjusted to obtain the best fit to the E_{OC} data. The calculated Z shows all the expected trends discussed above. The calculated Z vs. frequency is in good agreement with the E_{OC} curve of Figure 8 for all frequencies below ~ 5 kHz. At higher frequencies, however, the observed Z deviates from the model both in magnitude and in phase. This feature is likely to be an artefact, as it is not reproduced by EIS (ex-situ) measurements with simplified cell geometry. For instance, using a cell where the distance between the Zr working electrode and the counter electrode is reduced (~1 cm), and no capillary for the reference electrode in place, Z is observed to behave exactly as depicted in Figure 10 up to 1 MHz in frequency.

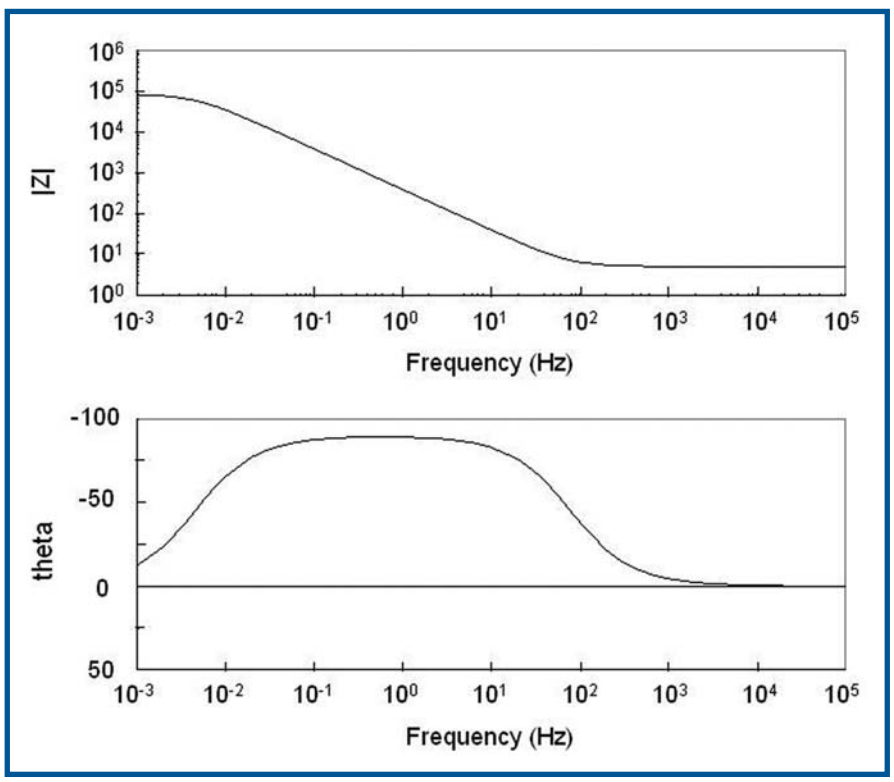

Fig. 10 The impedance of the proposed equivalent circuit whose parameters have been least-squares fitted to the EOC result depicted in Figure 8.

We are now ready to examine how NR and EIS could complement each other and lead to results that could not be obtained by using either of them alone. To this end, we need to first find correlations between the changes recorded by NR and EIS at various stages of the experiment. The E_{OC} curve of Figure 8 shows that, prior to anodization, the low-frequency $|Z|$ was very high, indicating the original passive oxide layer was continuous and provided good protection against corrosion. The high $|Z|$ persisted as we increased polarization to anodic potentials of 0 V, 0.5 V and 1 V (only 1 V curve is shown in Figure 8 for clarity). At the next higher potential, 1.5 V, the low-frequency $|Z|$ suddenly dropped and never recovered. As the 1.5 V curve is similar to the 3 V curve, only the latter is shown in Figure 8. The oxide layer thickness determined by NR, on the other hand, increased monotonically with the potential as shown in Figure 11. Note that there is no discernable discontinuity or anomaly of the oxide thickness at or around 1.5 V. It turned out that the expected discontinuity occurred for the SLD of the oxide layer. While the oxide SLD decreased with every potential increase (as seen in figure 7), the

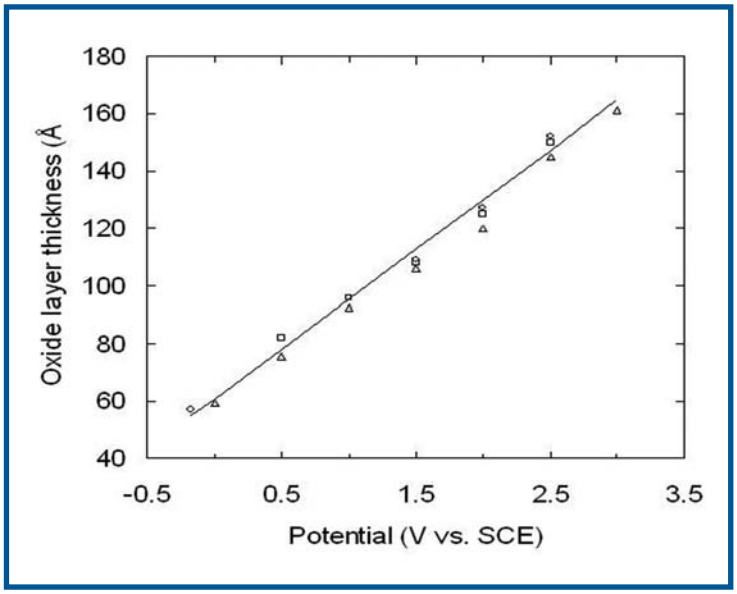

Fig. 11 Chronological variation of oxide layer thickness observed by neutron reflectometry at EOC (–0.17 V), and at set anodic potential increased in steps from 0 to 3 V at intervals of 0.5 V. Time sequence of repeated scans at a given potential is denoted by triangles (Δ), squares (□), and circles (o).

largest drop occurred for the potential increase from 1 to 1.5 V. Moreover, the second largest drop of oxide SLD occurred for the next potential increase, from 1.5 to 2 V. Higher subsequent potentials brought about further decreases of the oxide SLD but they were all very small. The explanation that is consistent with both the EIS and NR observations is that a significant number of cracks developed within the oxide layer at 1.5 V, and they were immediately filled with H_2O. This inrush of water led to a step in the oxide SLD, as well as a large drop in R_{ox} as even a few saline water pathways can effectively short-circuit the oxide capacitor.

A more detailed inspection of Figure 11 reveals a trend that very convincingly demonstrates the reliability of the NR data. The figure shows the results obtained by repeated NR scans using different symbols; triangles (Δ) are yielded by the scans carried out immediately after potential increase, squares (□) by the subsequent scan, and circles (o) by yet another scan if carried out. Lapse time between these scans is typically 6 h. Circles are the best estimate we have for the equilibrium oxide layer thickness, *i.e.* the thickness we would get at infinitely long time. A circle represents the very first point of the plot at E_{OC} since the oxide layer does not thicken by just filling the cell. Thus chronologically encoded, the plot shows a remarkable trend – the change is monotonic with the symbols appearing always in the order Δ, □, o. This shows that the variation of d_{ox} detected by NR are real, even when the thickening is only a matter of a few Angstroms (between □ and o).

Unexpectedly, the above monotonic trend revealed an underlying difference between the behaviour probed by NR and EIS. The solid-state ion transport across existing oxide no doubt continues many hours after the anodization potential was set. The behaviour of the cell current monitored by EIS, on the other hand, is distinctly different: it shoots up at the moment of the application of the potential, but decays to a small value within minutes. Over longer periods stretching beyond the first hour, the current is either very stable or drifts slightly. The drifts, typically very slow (over tens of minutes), may be in either the positive or the negative direction. This behaviour of the cell current, thus, stands in stark contrast with the unidirectional thickening of the oxide layer.

In retrospect, the fact that NR and ESI expose different processes is not surprising. Anodization involves mass and/or charge transport between layers of the working electrode, arising from motion of neutral atoms, electrons or ions. Movement of neutral atoms is detected only by NR, electrons only by EIS, and ions by both. This is perhaps the most compelling reason for performing NR and EIS concurrently in the study of passive oxide layers.

REFERENCES

1. M. Faraday, *Experimental Researches in Electricity, Vol. 2*, pp. *234–239*, Dover Publications, Inc., New York, (1965); republication of the original publication by Richard & John Edward Taylor in 1844.
2. M. Faraday, *Lond. and Edinb. Phil. Mag.* **4**, 53 (1836).
3. H.H. Uhlig, "Passivity of Metals", in *Proceedings of the 4th International Symposium on Passivity*, pp. 24–25, R.P. Frankenthal and J. Kruger editors, Electrochem. Soc. Inc., Princeton, New Jersey (1978).
4. D.G. Wiesler and C.F. Majkrzak, *Physica* **B198**, 181–186 (1994).
5. D.G. Wiesler and C.F. Majkrzak, *Mat. Res. Soc. Symp. Proc.* **376**, 247–257 (1995).
6. J.J. Noël, B.M. Ikeda, N.H. Miller, S.R. Ryan, D.W. Shoesmith, S. Sunder and Z. Tun in *Surface Oxide Films*, Proceedings Vol. 96-18, pp. 246–257, J.A. Bardwell editor, Electrochem. Soc. Inc., Pennington, New Jersey (1996).
7. Z. Tun, J.J. Noël and D.W. Shoesmith, *Physica B Condensed Matter* **241-243**, 1107–1109 (1998).
8. Z. Tun, J.J. Noël and D.W. Shoesmith, *J. Electrochem. Soc.* **146**, 988–994 (1999).
9. See Tun *et al.* (1999) [Ref. 8] and references therein.
10. N. Khalil and J.S.L. Leach, *Electrochim. Acta* **31,** 1279–1285 (1986).
11. D.D. Macdonald, *J. Electrochem. Soc.*, **139**, 3434–3449 (1992).
12. P. Meisterhahn, H.W. Hoppe and J.W. Schultze, *J lectroanal. Chem.* **217**, 159–185 (1987).
13. Values of specific gravity for Zr, ZrO_2 (zirconia), and ZrO_2 (baddeleyite) are 6.49, 5.6, and 5.8 respectively, giving R_{PB} = 1.56 for zirconia and 1.50 for baddeleyite.